Yuan et al. *NPG Asia Materials* (2023) 15:40
https://doi.org/10.1038/s41427-023-00487-8

NPG Asia Materials

ARTICLE Open Access

Nowhere to run: oligo (p-phenylene vinylene) kills oral intracellular bacteria photodynamically

Lintian Yuan[1,2], Xuancheng Fu[3,4], Wen Yu[3], Huagen Wei[5], Fan dong[2,6], Ludan Zhang[2,7], Guiyan Wang[2,8], Huihua Dong[2,6], Fengting Lv[3] and Yuguang Wang[2,6]

Abstract

Bacterial infections pose a severe threat to human health due to the exacerbation of antibiotic resistance and intracellular bacterial infections. Research suggests that oligo(p-phenylene vinylene) (OPV), commonly employed in the manufacture of organic solar batteries, can help address this issue. This study demonstrates the ability of OPV to target and sterilize intracellular *Porphyromonas gingivalis* and methicillin-resistant *Staphylococcus aureus* (*MRSA*) photodynamically. Most notably, OPV specifically targets bacteria without affecting healthy cells under dark conditions. Its chemical composition includes a conjugated backbone and ionic imidazole side chains, which allow OPV to bind to cell membranes. Furthermore, dental blue light curing lamps may excite OPV. Compared with antibiotics and traditional photosensitizers, OPV proves to be a potentially superior solution to eradicate intracellular microbial infections, both in fundamental research and clinical applications.

Introduction

Bacterial infections can result in localized or systemic diseases that require substantial medical resources, particularly antibiotics. Drug-resistant bacterial infections have become a global public health concern[1,2]. In addition to antibiotic resistance, bacteria can parasitize cells, produce intracellular drug-resistant bacteria and evade host immune cells or antibiotic assaults[3] and can even act as a "Trojan horse" to induce secondary infections[4]. Currently, more than two-thirds of prescription antibiotics are ineffective against intracellular infections, and higher concentrations of antibiotics to kill intracellular bacteria easily induce drug resistance[5].

Porphyromonas gingivalis (*P. gingivalis*) is a gram-negative anaerobic bacterium that can invade a variety of oral cells to cause periodontal disease[6,7]. Methicillin-resistant *Staphylococcus aureus* (*MRSA*), a gram-positive bacterium, is difficult to eliminate in wisdom tooth pericoronitis[8] and dry socket[9] and can even hide in normal tissues[10] to cause "*Staphylococcus aureus* bacteremia", which can be fatal[11,12].

Antibacterial photodynamic therapy (aPDT) has been used as a strategy to kill germs by incubating exogenous photosensitizers with bacteria, and toxic reactive oxygen species (ROS) are generated by sensitizing the surrounding molecular oxygen after light irradiation[13,14]. aPDT has several advantages over traditional therapies, including its noninvasiveness, high temporal and spatial resolution, and lack of drug resistance[15,16]. However, photosensitizers have difficulty rupturing cell membranes and entering cells, which makes it difficult for them to contact and kill bacteria in cells[17–19], and they can damage host cells[20]. Enabling photosensitizers to infiltrate cells and successfully kill intracellular drug-resistant bacteria is a challenging issue that must be solved.

Organic semiconductor materials have achieved notable prominence across a range of industrial, military, and biomedical sectors. These applications include but are not limited to organic solar cells, optical communication,

Correspondence: Fengting Lv (lvft@iccas.ac.cn) or
Yuguang Wang (wangyuguang@bjmu.edu.cn)
[1]Department of General Dentistry, Peking University School and Hospital of Stomatology, 100081 Beijing, P. R. China
[2]National Center for Stomatology & National Clinical Research Center for Oral Diseases & National Engineering Research Center of Oral Biomaterials and Digital Medical Devices, 100081 Beijing, P. R. China
Full list of author information is available at the end of the article

biosensors, combinational phototherapy, and photoactivatable protherapeutics[21–26]. Oligo(p-phenylene vinylene) (OPV) is an organic semiconductor material composed of a conjugated backbone and ionic imidazole side chains, which have an affinity to the cell membrane due to their molecular charge distribution and amphiphilic characteristics[27]. OPV, once utilized to make organic solar cells[28,29], was explored as an "electrochemiluminescence" or "photodynamic" method to kill *E. coli*[30] or fungi[31], and *E. coli*-bound OPV-conjugated backbones with drugs were used to kill tumor cells[32]. Additionally, OPV could be chemically linked with paclitaxel to form "chemical locks" to enhance anticancer drug uptake and reduce resistance[33]. Given that OPV can enter cells even after being modified[34,35], it is believed that OPV could be used to efficiently kill intracellular bacteria alone.

As illustrated in Scheme 1, when normal cells are exposed to bacterial contamination, they transform into infected cells. Despite the effects of immune cells and antibiotics, intracellular bacteria commonly persist as chronic infections, leading to further cell contamination. However, OPV has the unique ability to attach to both extracellular and intracellular bacteria. The application of blue light effectively eradicates the bacteria, allowing other normal cells to proliferate unhindered.

In this synthesis of OPV, the reactants underwent a series of reactions and purifications, including bromination, palladium-catalyzed coupling, and vinyl-tributyltin addition. The final product was a bright yellow compound, which was further processed and refluxed with N-methyl-imidazole to yield the orange powdered solid OPV. In this study, researchers designed experiments to evaluate the effectiveness of OPV as a potential antimicrobial agent against *P. gingivalis* and *MRSA*. The experiments included bacterial and cell cultures, OPV preparation and characterization, molecular dynamics simulation, excitation/emission peak detection, photobleaching, ROS generation, hemolysis, zeta potential and flow cytometry measurements, cytotoxicity testing, temperature safety testing, extracellular and intracellular bacteria killing experiments, morphological observation, and in vivo and ex vivo animal experiments.

Material and methods

We conducted a study on the photosensitizer OPV, which included the preparation and characterization of the compound. We also explored the use of OPV in antimicrobial photodynamic therapy (aPDT) using bacterial culture and cell culture experiments. Molecular dynamics simulations were carried out to investigate the mechanism of action of OPV. Additionally, we performed various experiments to test the efficacy and safety of OPV, including photobleaching, ROS generation, hemolysis, cytotoxicity, temperature safety, extracellular sterilization, and tests of the intracellular bacteria-killing efficiency of OPV.

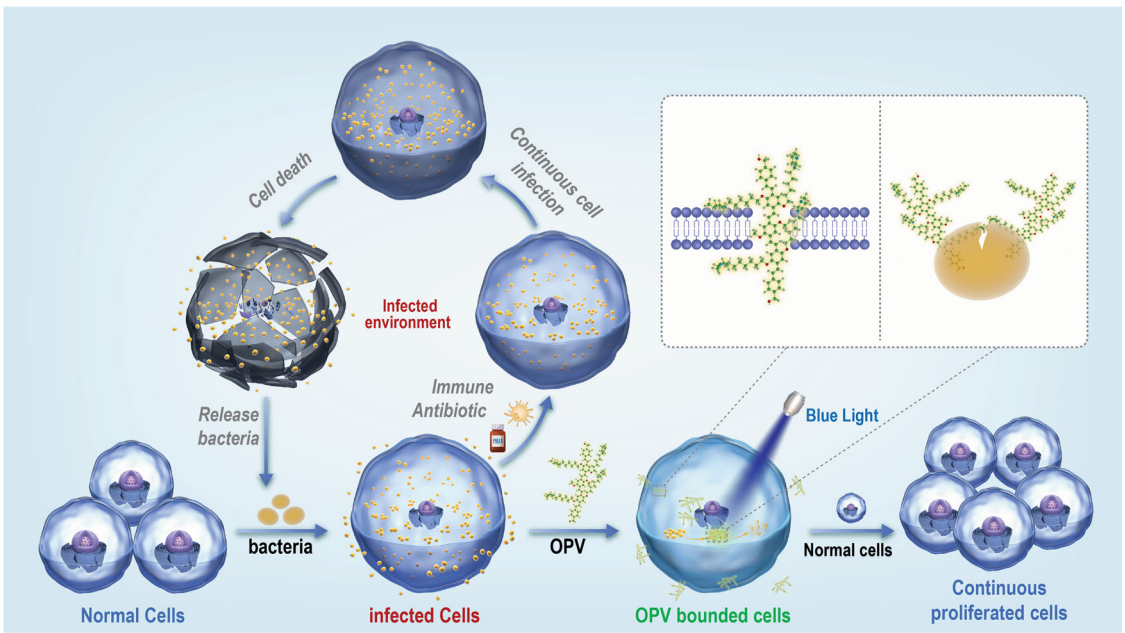

Scheme 1 The mechanism by which OPV enters cells and kills intracellular bacteria. As a photosensitive membrane insertion molecule, OPV can photodynamically kill bacteria while also preventing regrowth and secondary infection.

Bacterial culture

P. gingivalis (W83) and self-luminous *MRSA* (ATCC 33591) were obtained as gifts from the Central Laboratory of Peking University School and Hospital of Stomatology and Shanghai No.9 People's Hospital, Shanghai Jiao Tong University School of Medicine, respectively. *P. gingivalis was* grown on 5% sheep blood BHI agar (A8190, Solarbio, Beijing, China) containing 5 μg/mL hemin (H8130-1G, Solarbio, Beijing, China) and 1 μg/mL vitamin K (V8150, Solarbio, Beijing, China) or liquid BHI medium containing hemin and vitamin K, both in anaerobic cultivation (C-1, AnaeproPack, MGC, Tokyo, Japan). *MRSA* was grown on BHI agar or BHI liquid medium. The bacterial solution was incubated overnight at 37 °C with shaking at 180 rpm, and then the final concentration of bacteria was adjusted to OD630 nm = 0.1. *P. gingivalis*: 10^9/mL, *MRSA*: 10^8/mL in PBS by absorbance reader (CMax Plus, Molecular Devices, San Jose, USA).

Cell culture

HaCaT cells were generous gifts from the Department of Oral and Maxillofacial Surgery of Peking University School and the Hospital of Stomatology. The *HaCaT* cell line is an epithelial cell line widely used in studying biological processes related to the skin, such as skin infections. In aPDT, *HaCaT* cells were used to evaluate the biocompatibility and cytotoxicity of photosensitizers and as an in vitro model to study the antimicrobial mechanism of this therapy[36–38]. The cells were cultured with phenol red-free DMEM (containing 10% FBS, 100 U/mL penicillin and 100 μg/mL streptomycin), and the medium was refreshed every 2 days.

OPV preparation and characterization

The reaction mixture was stirred for 3 days in a flask containing 1.7 g (5.43 mmol) of 4-bromo-2,5-dihydroxyiodobenzene, 70 mL of degassed acetone, 5.6 g of K_2CO_3, 140 mg of 18-crown-6, and 20 g (82 mmol) of 1,6-dibromohexane. The residue obtained after filtration was purified through silica gel chromatography. Subsequently, 10 mg of acetate palladium, 25 mg of tri-o-tolylphosphine and 600 μL of tributylamine were added to the purified compound (300 mg, 2.3 mmol) and 4.2 g (6.5 mmol) of (4-vinylphenyl) methanol in degassed toluene. The resulting mixture was stirred at 80 °C for 24 h, and the residue was purified by silica gel chromatography.

A total of 800 mg (1.25 mmol) of the product obtained earlier was dissolved in 50 mL of degassed toluene to which 1 g (6 mmol) of tributyl(vinyl)tin and 20 mg of tetrakis(triphenylphosphine)palladium were added. The mixture was stirred at 100 °C for 12 h, after which the residue was purified with silica gel chromatography to obtain a bright yellow solid. To 5 mL degassed toluene containing 190 mg (0.32 mmol) of the bright yellow compound, 52 mg (0.13 mmol) of 1,4-diiodo-2,5-dimethoxybenzene, 10 mg of acetate palladium, 20 mg of tri-o-tolylphosphine, and 100 μL of tributylamine were added under a nitrogen atmosphere. The resulting mixture was stirred for 2 days, and the residue was purified by silica gel chromatography to obtain a bright yellow solid compound.

The purified compound was dissolved in 10 mL of acetone, and 150 mg of sodium iodide was added to the solution, followed by 30 mL of CHCl3 to extract the desired product. The product was OPV as a bright yellow solid. Finally, 136 mg (1.66 mmol) of N-methylimidazole was added to 125 mg (0.083 mmol) of the orange powder solid product, which was dissolved in 10 mL of acetonitrile. The resulting mixture was refluxed for 24 h. After removing the solvent and N-methylimidazole under vacuum, the oily red residue was washed with 20 mL of ethyl acetate to obtain the desired orange powder form of OPV[31].

Molecular dynamics simulation

GROMACS 2020.6[39], Visual Molecular Dynamics[40], AutoDock vina V1.1.2[41] and Discovery Studio v4.5 (BIOVIA, San Diego, CA, USA) were used for molecular docking between OPV and POPG and molecular simulation between OPV and POPC.

The MD simulations were performed with the GROMACS package, version 2019.6[42]. The SPC water model was selected to simulate the aqueous solution environment[43]. POPC (1-palmitoyl-2-oleoyl-sn-glycero-3-phosphocholine) bilayers were chosen to mimic the cell membranes, and there were 400 lipid molecules for each membrane model. The lipid molecules utilized Kukol parameters[44]. The topology files of OPV and VAN were generated from the ATB website[45].

POPC bilayers were set up as follows. The lipid molecules were modeled in a periodic box (16 × 17 × 15 nm) and were solvated with SPC water. For this neutral system, counter ions were not needed. Two rounds of energy minimizations using steepest descent and conjugate gradient algorithms were successively carried out on the water molecules. Then, position-restrained MD simulations were performed for each system, in which the positions of lipids were restrained under constant particle number, pressure and temperature (NPT) conditions with a Nosé–Hoover thermostat[46] and Parrinello-Rahman barostat[47] (1 atm). During position-restrained MD simulations, the temperature was gradually increased to 298.15 K. Afterward, 100 ns simulations were performed without any constraints for the system to make lipids adapt to the simulation condition, and the last conformation was used for the subsequent simulations of small molecule transmembrane.

For simulations of small transmembrane molecules, OPV or VAN was placed above the membrane surface at a

distance of approximately 0.5 nm. The OPV/VAN-POPC system was placed in a periodic box (16 × 17 × 15 nm). The box was filled with SPC water. Counter ions were added to neutralize the net charge of the system. The energy minimizations followed by position-restrained simulations were performed in the same way as POPC bilayer simulations. For each system, position-restrained equilibration simulations were performed for 1000 ps in the NPT ensemble, and the temperature was gradually increased to 298.15 K. Then, another equilibration simulation was performed for 1000 ps in the NPT ensemble under constant temperature (298 K) and pressure (1 atm) with a Nosé–Hoover thermostat and Parrinello-Rahman barostat. Afterward, full MD simulations without any position restraints were carried out for OPV/VAN-POPC for 10 ns. The last snapshot of the system was used for steered molecular dynamics simulations. OPV/VAN was pulled away along the *z*-axis (Supplementary Fig. S1) over 1000 ps using a spring constant of 1000 kJ/mol/nm^2 and a pull rate of 0.01 nm/ps. Configurations for the umbrella sampling were generated from before steered molecular dynamics simulation trajectories described in this paper[48–50].

The sampling distance was from approximately 1.0 to 11.0 nm along the *z*-axis, using approximately 0.2 nm spacing. Finally, 54 windows were generated, and in each window, 10 ns of MD was performed. Analysis of the results was performed with the weighted histogram analysis method (WHAM) using GROMACS2019.6[51].

The molecular docking process was carried out as already described[52]. Using AutoDock Vina 1.1.2, two molecules were docked with OPV to examine their binding mode. ChemBio3D Ultra 14.0 was used to transform the two-dimensional (2D) structures of the POPG molecules into three-dimensional (3D) structures after they were downloaded from PubChem (https://pubchem.ncbi.nlm.nih.gov/). POPG was selected as the receptor, and the OPV molecule was selected as the ligand. The docking input files were produced using the AutoDock Tools 1.5.6 package. The dimensions of the sizes x, size y, and size z of the POPG's search grid were determined to be center x: 0.711, center y: −1.37, and center z: 1.224. The ideal binding method was chosen for additional examination. PyMol 2.5 (www.pymol.org) and Discovery Studio v4.5 (Accelrys Software, Inc., San Diego, CA, USA) software were used.

Excitation/emission (Ex/Em) peak detection

To find a suitable light source to excite OPV, the Ex/Em peak of OPV (5 μM) was tested by a microplate detector (Enspire, PerkinElmer, USA, Waltham, Massachusetts). The Ex-light sources were 405, 450, 470, 520, 565, 635, 660, and 808 nm, and the Em-wavelength was the Ex-wavelength added at 20 nm up to 750 nm.

Photobleaching

OPV (5 μM) photosensitizer photobleaching with a light source (470 nm, 50 mW/cm^2, M470L4, Thorlabs, Newton, New Jersey, USA) in 0–5 min was detected by Enspire in the wavelength range of 300–540 nm.

ROS experiment

Reactive oxygen species (ROS) of OPV (5 μM) were evaluated by DCFH (5 μM). The fluorescence spectrum was measured after blue light (470 nm, 5 mW/cm^2) for 5 min. It was recorded in the emission range of 510–700 nm with an excitation wavelength of 488 nm.

Hemolysis

The hemolytic effect of OPV was examined by incubation with mammalian blood based on a previously published method[53]. The defibrinated sheep blood (TX0030, Solarbio, Beijing, China) was washed with phosphate-buffered saline (PBS, P1010, Solarbio, Beijing, China) and centrifuged (9000 × *g*, 3 min) in a 1.5 mL centrifuge tube to prepare sheep red blood cells (RBCs). OPV (5 μM) compared with antibiotics (gentamycin, metronidazole, vancomycin, 50 mg/mL) and PBS and water. A 50% volume of RBC suspension was added to each tube, mixed with different samples, and then incubated for 3 h at room temperature in the dark to detect the absorbance of the different groups at 400–700 nm.

Zeta potential and flow cytometry

For each experimental trial, *MRSA* or *P. gingivalis* bacteria were incubated with either PBS or OPV (5 μM) for 30 min at room temperature. Once complete, the samples were analyzed using a Zetasizer (Nano ZS90, Malvern, London, UK) or flow cytometer (NovoCyte, Agilent, Santa Clara, USA) with a 488 nm wavelength.

Cytotoxicity

For the live and dead cell staining experiment, live and dead cell staining and the CCK-8 cell viability test were used to test the cytotoxicity of OPV. *HaCaT* cells were cultured in a 12-well plate at 10^5/mL. When cell confluency reached 60–80%, PBS or OPV (6 μM) with blue light (470 nm, 50 mW/cm^2, 0, or 2 min) was added. After illumination, 1.5‰ calcein-AM/PI stain (CA1630, Solarbio, Beijing, China) was added for 30 min for observation with a fluorescence microscope (CKX53, Olympus, Tokyo, Japan). The same method of culturing cells in 96-well plates was used, and OPV (0–6 μM) was added with illumination (470 nm, 50 mW/cm^2, 0 or 2 min). Then, 100 μL of 10% CCK-8 was added to each well and cell-free well (blank group), and the cells were incubated for 30 min with a microplate reader at an OD_{450} nm. The cell viability of the treated wells was calculated and compared to that of the untreated cells (100%).

Temperature safety

To ensure that OPV with blue light would not cause obvious heat damage to normal cells, 5 mL PBS and OPV (5 μM) were placed into a 2 mL EP tube. With infrared camera observation, the temperature change of PBS and OPV in blue light (470 nm, 50 mW/cm^2, 0–5 min) was recorded.

Extracellular sterilization

MRSA or *P. gingivalis* suspensions of 200 μL/well in 48-well plates were added to different drugs as follows: OPV (0–5 μM) with 470 nm light at 50 mW/cm^2 for 0 or 2 min. Each sample was serially diluted from 10^1 to 10^6 in agar plates for the CFU assay.

Intracellular sterilization

HaCaT cells were incubated to 60–80% confluence in a 12-well plate, and a final concentration of 10^8/mL *P. gingivalis* and 10^6/mL *MRSA* bacteria was added for 12 or 4 h, respectively, in DMEM. Then, *HaCaT* cells were washed five times with PBS and incubated with DMEM containing gentamycin (50 μg/mL) for 2 h to inhibit extracellular bacteria. PBS, OPV (5 μM), vancomycin (50 μg/mL, in the *MRSA* group) or metronidazole (50 μg/mL, in the *P. gingivalis* group) was added to each well, incubated for 20 min and then exposed to 470 nm light for 0 or 2 min. After that, each sample was washed with PBS three times to remove the drugs, and the cells were lysed with 200 μL water for 10 min. Then, the cells were further scraped off by a cell scraper and tested by CFU assay from a cell suspension containing intracellular bacteria. The counting method was the same as before. The LIVE/DEAD BacLight Bacterial Viability solution (L7012, Invitrogen, Thermo Fisher, Carlsbad, USA) was used to observe *HaCaT* cytotoxicity with intracellular bacteria in different drugs. The intracellular bacterial incubation methods were as previously described. After adding PBS, antibiotics (vancomycin and metronidazole 50 μg/mL) or OPV (5 μM) for 30 min, the solution was refreshed with saline, and SYTO 9 and PI (1.5‰, in saline solution) were used to observe the cells under a fluorescence microscope.

Morphological observation

The cells were cultured in a glass-bottomed confocal culture dish, and the experimental culture method of intracellular bacteria was the same as before. After fixation with 4% paraformaldehyde for 30 min, OPV (5 μM) (green), DiD stain (red, D4019, Us Everbright, Suzhou, China), and Hoechst 33258 stain (blue, C1022, Beyotime, Shanghai, China) were used for observation under a confocal microscope (LMS710, Zeiss, Tokyo, Japan). The DiD stain has far emission light than OPV, which could have less of a cross-color effect than other stains (such as Calcein-AM).

Animal experiment in vivo

All animal experiments were approved by the Medical Ethics Committee of Peking University Ethics of Laboratory Animal Welfare (LA2022477). BALB/c mice (female, 6–8 weeks, Charles River, $n = 3$). The back was shaved, and a punch (Φ: 3 mm) was used on the left and right sides of the back to make wounds. The punch tissues were collected for ex vivo experiments. The same amount of *MRSA* or *P. gingivalis* (108 CFU/mL, 10 μL) was added to the back wound. The next day, different wounds were randomly treated with the drug for 20 min as follows: (1) PBS (blank group), (2) Bacteria + PBS, (3) Bacteria + Vanco or Metro, (4) Bacteria + OPV, (5) Bacteria + OPV + light (470 nm, 50 mW/cm^2, 5 min). Wound sizes were recorded for 5 days.

Animal experiment ex vivo

An ex vivo experiment was used to ensure that OPV could bind tissues and inhibit intracellular bacteria. Animals were anesthetized, shaved, and 75% alcohol-coated on the surface to disinfect the back skin, and the same punch was used to obtain a piece of skin tissue (φ: 3 mm). Each tissue sample was washed at least three times with PBS, placed into a 0.2 mL EP tube and classified into five groups as described above, and *MRSA* or *P. gingivalis* (10^8 CFU/mL, 100 μL, 10 groups in total, repeated three times) was added and cultured overnight. Then, each sample was washed three times with PBS again and incubated with PBS containing gentamycin (50 μg/mL) for 2 h to inhibit extracellular bacteria. After that, different drugs were added and incubated (under the same conditions as in 2.1.5) for 20 min. Then, the BHI culture medium was incubated overnight to test if bacteria can be regrown from the ex vivo tissues.

Living fluorescence in vivo

To further demonstrate that bacteria were immediately damaged upon light exposure, 10 μL of *MRSA* solution was inoculated onto the backs of hairless mice. All other experimental details remained the same as before. An IVIS® Lumina III imaging system (PerkinElmer, Waltham, MA, USA) was then used for observation at the same location before or after illumination.

Animal safety

In addition, the heart, liver, spleen, lung, and kidney tissues of specific-pathogen-free mice were administered PBS and OPV locally for 5 days and then fixed with 4% paraformaldehyde. The toxicity of OPV was observed by histological hematoxylin and eosin (H&E) staining under a microscope.

Statistical analysis

All numerical data are expressed as the mean ± standard deviation. Intergroup differences were assessed using

repeated-measures ANOVA or one-way ANOVA when necessary. All statistical analyses were performed with Statistical Package for the Social Sciences (SPSS) 27.0 (IBM Corp., Armonk, NY, USA), and figures were created using Origin 2022 (OriginLab, MA, USA). Values of $p < 0.05$ were considered statistically significant (*$0.01 < p < 0.05$, **$0.001 < p < 0.01$, ***$p < 0.001$).

Results and discussion

We conducted experiments on OPV, a photosensitizer, and its interactions with bacterial membranes, as well as its phototoxicity and ability to kill bacteria. By using various methods and software, we were able to visualize the interactions between OPV and bacterial membranes and found that OPV can effectively bind to bacterial cell membranes. The results showed that there were no significant differences in zeta potentials after the addition of OPV and that OPV has good biocompatibility and blood circulation safety. Our study found that 470 nm blue light was the best excitation light source for OPV and that illumination times between 2 and 5 min were suitable for eliciting its photodynamic effect. Our experiments also showed that OPV has negligible cytotoxicity and significant bacterial killing abilities in suspension and intracellular environments when used with blue light.

Fundamental characteristics of OPV

To visualize the form of OPV insertion and crossing the cell membrane, molecular dynamics simulations of OPV interacting with 1-palmitoyl-2-oleoyl-sn-glycero-3-phosphocholine (POPC) membranes were studied by GROMACS[39] and visualized by the Visual Molecular Dynamics software package[40], as shown in Fig. 1A. Simulation images demonstrating the landing (i), anchoring (ii), submersion (iii), initial tunneling (iv), in which a charged side chain reaches the inner leaflet), membrane spanning (v), and full insertion (vi) of OPV. The detailed data are shown in Supplementary Figs. S1 and S2.

To visualize OPV binding to the membrane of *P. gingivalis*, AutoDock Vina v1.1.2[41] and Discovery Studio v4.5[54] were used to calculate the binding interactions between OPV and the bacterial membrane (L-α-phosphatidylglycerol, POPG) for visualization (Fig. 1B, Supplementary Table S1). OPV had nine structures that could bind to POPG, and the most suitable structure had an affinity energy of −3.6 kcal/mol. When the binding energy between the photosensitizer and POPG is less than −2.5 kcal/mol, the molecule is more likely to adsorb to the membrane surface[55,56], and the ROS produced upon illumination may act on the bacterial membrane.

Zeta potentials (ζ) were used to gain a better understanding of how OPV interacted with *MRSA* or *P. gingivalis*. There were no significant differences in these potentials for *MRSA* or *P. gingivalis* before and after the addition of OPV (Fig. 1C, and Supplementary Table S2), which revealed that OPV might insert into the bacterial cell membranes instead of forming electrostatic interactions. The absolute value of the zeta potential decreased because *P. gingivalis* itself has a strong gathering ability[57,58].

Although OPV was used topically, we also found that OPV (5 μM) did not trigger hemolysis. The hemolysis assay of OPV (5 μM) treated with red blood cells showed good biocompatibility, not significantly different from that of phosphate-buffered saline (PBS) or antibiotics (e.g., gentamycin, metronidazole, and vancomycin) (Fig. 1D and Supplementary Fig. S3). These results indicated that OPV, similar to other antibiotics, has good blood circulation safety. Therefore, when OPV is used in local infections, it would be a safe method.

Based on our previous results, OPV had broad absorption (e.g., 350–550 nm) of white light[31]. To find a more suitable light source, wavelengths ranging from 405 to 808 nm were used to excite OPV, and it was determined that light sources of 405, 450, and 470 nm could excite OPV and that the peak emission wavelength was approximately 550 nm (Fig. 1E). Light with a frequency higher than 520 nm has a minor impact on OPV, whereas wavelengths below 450 nm may pose more harm to cells and fail to penetrate deep into the skin[59]. However, 470 nm light may be less cytotoxic and penetrate deeper into tissues and has been used for neonatal jaundice[60]. Studies have shown that irradiation with 470 nm blue light does not affect wound healing, and low doses of blue light (5 J/cm^2) may promote protein synthesis. It has also been found that the effect on fibroblast integrity is safe when the dose is under 110 J/cm^2 [61]. Our study used a maximum dose of 50 mW/cm^2 of 470 nm blue light, and an exposure of 5 min was equivalent to 15 J/cm^2, which falls within the safe range of light exposure dosage. Hence, 470 nm was selected as the excitation light source.

Considering that the illumination time could cause a photobleaching effect on the OPV, to find a suitable illumination time, blue light (470 nm, 50 mW/cm^2) was administered as the excitation light with durations of 0 to 5 min. After 1 min of illumination by blue light, the absorption peak of OPV was reduced by approximately 70%. When illuminated for 2–5 min, the fluorescence intensity of the remaining fluorescence was less than 10% (Fig. 1F). Therefore, the photosensitizer selected in this study was illuminated for a duration of 2–5 min.

The photodynamic effect of OPV was observed using the ROS detection agent DCFH, and it was found that OPV could produce ROS when 470 nm blue light was used (Fig. 1G, H). According to the results, it reached nearly the maximum at the 4- to 5-min duration and reached nearly 70% efficiency for 2 min. Considering the

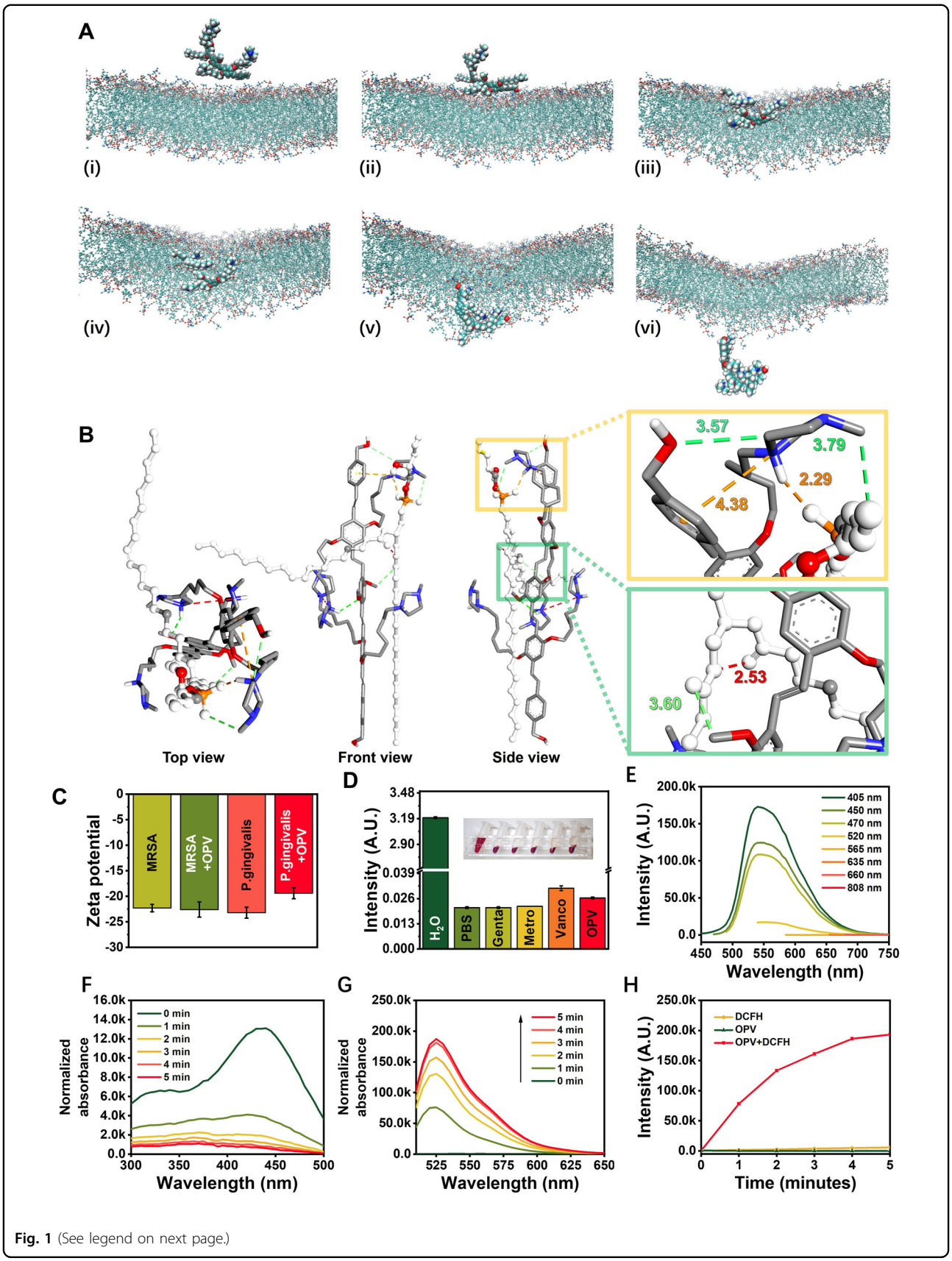

Fig. 1 (See legend on next page.)

(see figure on previous page)
Fig. 1 Fundamental characteristics of OPV. A GROMACS and Visual Molecular Dynamics software simulating the entry of OPV into the cell membrane (POPC) from 0 to 1 ns. Surrounding ions and water molecules are not shown (Diameter σ = 8.5 Å.) **B** The interactions between OPV and the bacterial cell membrane (POPG), as determined by AutoDock and Discovery Studio software. The length of binding: Dark green: hydrogen bond, light green: hydrocarbon, yellow: electrostatic bonds. **C** Zeta potentials of *MRSA* or *P. gingivalis* with or without OPV. **D** Hemolysis test of water (H_2O), PBS, gentamycin (genta), metronidazole (Metro), vancomycin (Vanco), and OPV on sheep red blood cells. **E** Emission peak curve of OPV excited by light with different wavelengths. **F** 470 nm light source (50 mW/cm^2) after OPV irradiation for 0–5 min; the absorption of 300–500 nm light decreases. **G** DCFH detects the generation of total ROS by OPV excited by a 470 nm laser and **H** DCFH, OPV, OPV+DCFH emission peak (ex/em:488/525 nm) from 0 to 5 min.

photobleaching results and comfort considerations in clinical practice, 2–5 min could be a suitable time.

Cytotoxicity experiment

To determine the phototoxicity of OPV to cells, live/dead cell stains (e.g., calcein-AM and PI) were evaluated with fluorescence microscopy and CCK-8 assays with a microplate reader. In the staining experiment, there was no substantial toxicity of OPV exposed to light (470 nm, 50 mW/cm^2, 2 min) to *HaCaT* cells (Fig. 2A, B). The CCK-8 assay found that OPV (0–6 μM) exposed to light (470 nm, 50 mW/cm^2, 2 min) had no significant cellular toxicity or phototoxicity (Fig. 2C). When cells were incubated with bacteria, the killing ability of OPV against bacteria was much greater than that against cells (Fig. 2D, E). Additionally, to ensure that OPV (5 μM) and blue light do not produce obvious heat effects, the temperature safety was measured with an infrared thermal camera (Supplementary Fig. S4). Both the PBS and OPV (5 μM) groups showed no obvious temperature changes during blue light illumination (470 nm, 50 mW/cm^2, 5 min). Moreover, OPV had lower cytotoxicity than Ce6 and vancomycin or metronidazole when administered to *HaCaT* cells contaminated with *MRSA* or *P. gingivalis* (Supplementary Fig. S5). Combined with our previous research results[31], OPV used with blue light (470 nm, 50 mW/cm^2, 2 min) also had negligible cytotoxicity to uncontaminated or contaminated cells.

Bacterial suspension experiment

The killing effects of OPV on *MRSA* or *P. gingivalis* in suspension were examined using various OPV concentrations and illumination times. The results revealed that with 470 nm illumination at 50 mW/cm^2 for 2 min, 5 μM OPV could kill *MRSA* and *P. gingivalis*, as determined by colony-forming unit (CFU) tests (Fig. 3A–C). *P. gingivalis* is a gram-negative bacterium that has an impermeable outer cell membrane to block antibiotics and photosensitizers and protect it from being sterilized, but OPV still sterilized up to 10^6 CFU/mL *P. gingivalis* under light. However, traditional photosensitizers, such as methylene blue, toluidine blue O and indocyanine green, killed fewer than 10^1 CFU/mL at similar drug concentrations[62]. Additionally, live/dead bacterial staining by fluorescence microscopy (Fig. 3D) indicated that the bacterial cell membrane was nearly destroyed when OPV was illuminated, while the other groups showed little damage. Scanning electron microscopy (SEM) showed that both *MRSA* and *P. gingivalis* cell membranes were damaged under light (Fig. 3E).

Intracellular bacteria observation and killing

Transmission electron microscopy (TEM) imaging of bacteria-infected *HaCaT* cells showed that *MRSA* and *P. gingivalis* could be maintained in the *HaCaT* cells (Fig. 4A, B).

A confocal laser scanning microscope (CLSM) was used to observe OPV binding to intracellular *MRSA* or *P. gingivalis* in *HaCaT* by using the following stains: nucleus (Hoechst 33258, blue); cell membrane (DiD, red); and OPV (green) (Fig. 4C, D). From the perspective of the number of OPV-binding bacteria, flow cytometry (FCM) methods showed that 97.75% of *MRSA* were strongly positively bound to OPV, while 81.14% of *P. gingivalis* were positively bound with OPV (Fig. 4E, F). As described above, *P. gingivalis*, as a gram-negative bacterium, contains a lipopolysaccharide in the outer membrane and can resist the penetration of OPV better than gram-positive bacteria. Therefore, the OPV fluorescence intensity in *MRSA* was higher than that in *P. gingivalis*.

MRSA and *P. gingivalis* were cocultured with *HaCaT* cells for colony-forming unit (CFU) tests. Compared with PBS or antibiotics, OPV can clearly sterilize intracellular *MRSA* or *P. gingivalis* structures. The results showed that 5 μM OPV used with 50 mW/cm^2 of 470 nm light for 2 min could also kill *MRSA* or *P. gingivalis* intracellular bacteria, based on the results of CFU tests (Fig. 4G, I) and quantitative evaluations (Fig. 4H, J). In our study, the antibiotics vancomycin and metronidazole (50 mg/mL) had no obvious bactericidal effects. Previous studies have shown that the antibiotic concentrations necessary to treat intracellular bacteria often need to be increased by 100-fold to achieve similar inhibition to the effects on extracellular bacteria[63].

Animal experiments

Wound experiment

In the in vivo experiment (Fig. 5A), different treatments were applied to the back wounds of mice infected with

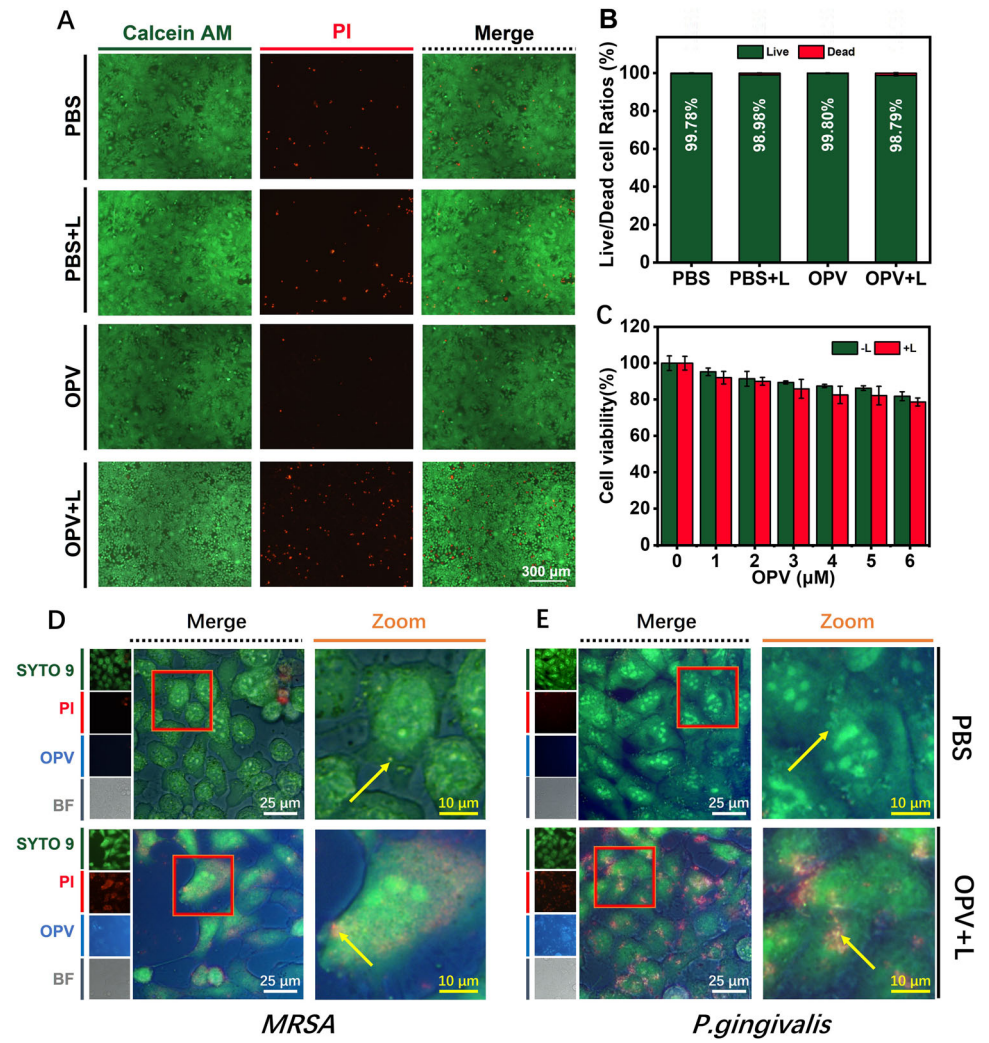

Fig. 2 OPV cytotoxicity test. A Live and dead cell stains, Calcein-AM (green) and PI (red) were used to observe the phototoxicity of OPV on *HaCaT* cells under a fluorescence microscope. **B** Quantitative evaluation of the toxicity of PBS and OPV to *HaCaT cells* of (**A**). **C** CCK-8 detected OPV (0–6 μM) in *HaCaT* cells under dark and light conditions. **D**, **E** SYTO 9 (green) and PI (red) were used to observe the phototoxicity of OPV (blue) on *HaCaT* cells or bacteria (yellow arrow, *MRSA* or *P. gingivalis*) under a fluorescence microscope.

MRSA or *P. gingivalis* (Fig. 5B–E). This study created identical wounds on the back of the same animal, which allowed better comparison and observation of wound recovery, reduced the number of animals used, and complied with the principles of "reduction," "replacement," and "refinement" in animal ethics[64]. In terms of statistical analysis, the principle of repeated-measures ANOVA was used, which analyzes the results of multiple measurements of the same experimental unit (such as the same animal), eliminates the influence of individual differences on the experimental results and improves the reliability and accuracy of the experiment. In this study, the same animal's five wounds on the back were the same experimental unit, and different drugs were the conditions for multiple measurements. Therefore, repeated-measures ANOVA is suitable for this situation and can detect whether the different drugs have a significant effect on the healing speed of different wounds on the same animal.

The results of the *MRSA* group showed that different drug treatments had a significant effect on wound size ($F = 218.861$, $p < 0.001$) (Supplementary Table S3). On the fifth day, the wound size in the OPV+L group was significantly reduced compared to that in the PBS group ($p < 0.001$) and less greatly reduced compared to that in the Vanco group ($0.001 < p < 0.05$). Therefore, the OPV+L treatment was the most effective. There was no significant difference in wound area between the OPV group and the PBS group ($p > 0.05$) (Supplementary Table S4).

The results of the *P. gingivalis* group showed that different drug treatments had a significant effect on wound

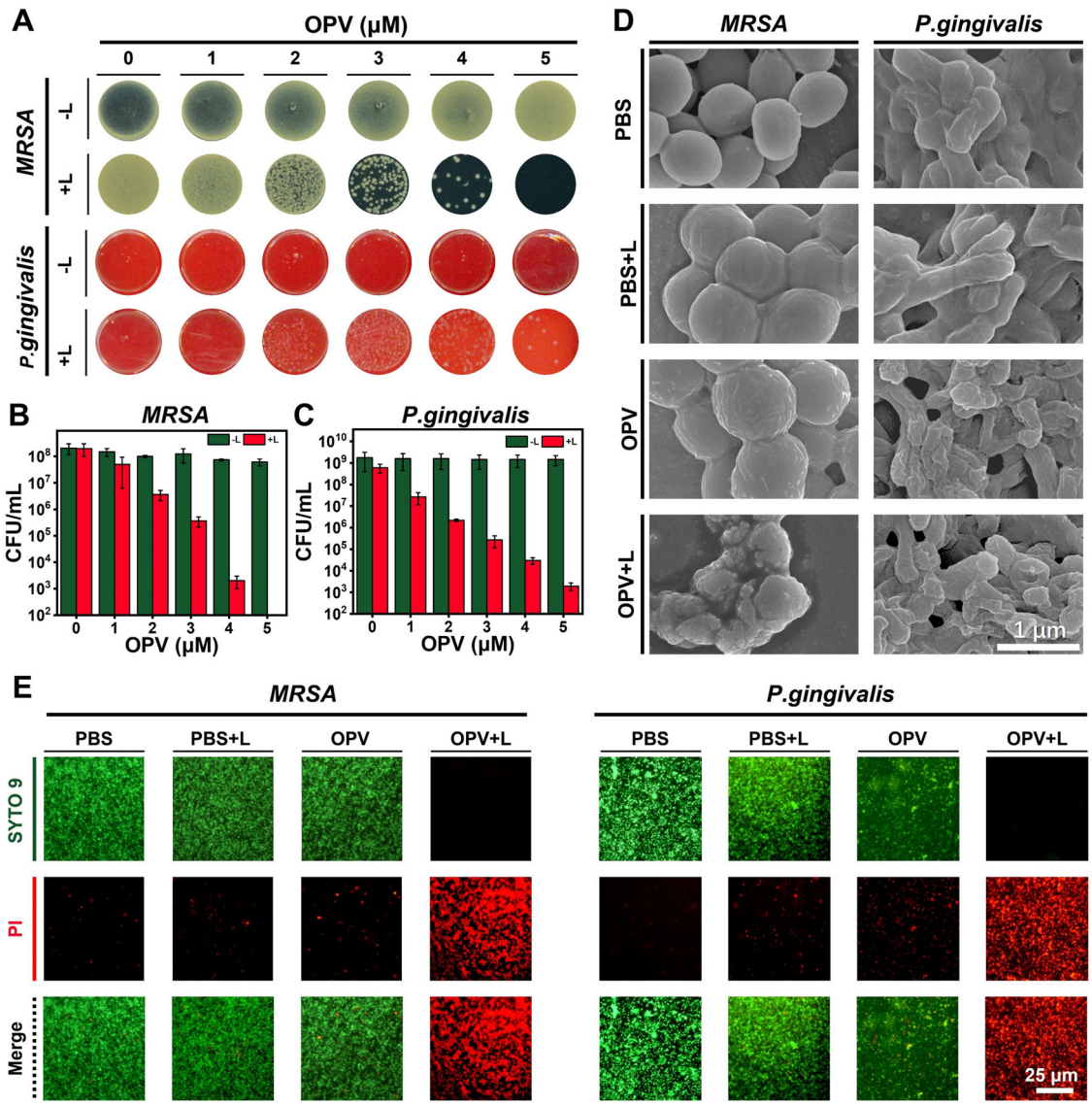

Fig. 3 The bactericidal effect of OPV on suspended bacteria. A The dark toxicity and phototoxicity (470 nm, 50 mW/cm^2, 0 or 2 min) of OPV to *MRSA* and *P. gingivalis*-suspended bacteria at different concentrations in CFU plates and **B**, **C** their quantitative evaluation. **D** SEM observation of OPV killing of *MRSA* and *P. gingivalis* cell membranes. **E** Fluorescence microscopy observation of OPV killing suspended bacteria stained by SYTO 9 (green) and PI (red).

size ($F = 109.442$, $p < 0.001$) (Supplementary Table S5). On the fifth day, the wound size in the OPV+L group was significantly reduced compared to that in the PBS group ($p = 0.013 < 0.05$) and less greatly reduced compared to that in the Vanco group ($p = 0.017 < 0.05$). There was no significant difference in wound area between the OPV group and the PBS group ($p > 0.05$) (Supplementary Table S6).

Ex vivo experiments

Ex vivo experiments could further explain why OPV could attach to tissues. After a tissue sample was obtained, it was cultivated with *MRSA* or *P. gingivalis* to provide different treatments (e.g., PBS, OPV with or without light irradiation, vancomycin, and metronidazole) (Fig. 5F). We observed the light density of the bacteria from incubation and polluted the medium from the infected tissue under different treatments (Fig. 5G, H).

The ex vivo experiments of this study aimed to evaluate the effectiveness of OPV in binding tissues and inhibiting intracellular bacteria. One-way ANOVA was employed to compare the means of different treatment groups for data analysis. Levene's test was conducted to assess the homogeneity of variances, and the significance level was

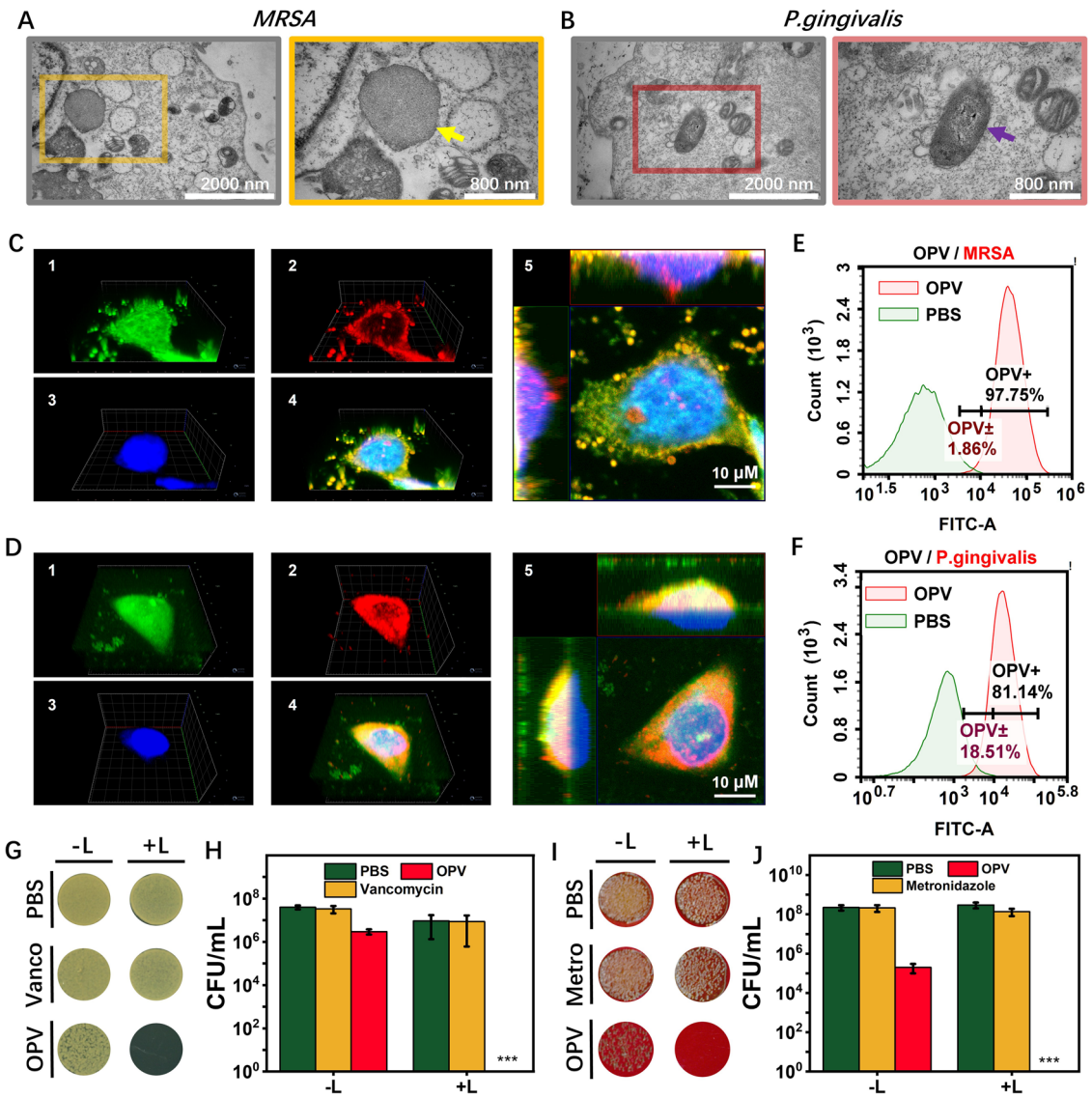

Fig. 4 OPV binding and killing effect on intracellular bacteria. A, **B** TEM images confirmed the existence of intracellular bacteria in *HaCaT* cells. Yellow arrow: *MRSA*, purple arrow: *P. gingivalis*. **C**, **D** Confocal image of OPV (green) and intracellular *P. gingivalis* or *MRSA* with DiD staining (red) and cell nuclei with Hoechst 33258 staining (blue) in 3D view. **E**, **F** Flow cytometry was used to observe the binding of OPV with *MRSA* and *P. gingivalis*. The positive OPV combined with bacteria named "OPV+" with black words and the deep red words "OPV±" mean OPV weakly positive binding to bacterium. **G**, **H** The bactericidal effect of OPV on intracellular *MRSA* by PBS and vancomycin (Vanco). **I**, **J** The bactericidal effect of OPV on intracellular *P. gingivalis* by PBS, metronidazole (Metro) and OPV (*0.01 < p < 0.05, **0.001 < p < 0.01, ***p < 0.001).

set at 0.05, indicating the presence of heterogeneity of variances. Hence, the Games-Howell post hoc test, which is a conservative test that does not assume equal variances and is suitable for small sample sizes, was used for pairwise comparisons.

In the *MRSA* experiment, the results of Levene's test showed significant heterogeneity of variances in the *MRSA* group ($p = 0.017$, Supplementary Table S7). ANOVA results indicated significant differences between treatment groups ($F = 520.080$, $p < 0.001$, Supplementary Table S8). The post hoc test using Games-Howell showed significant differences between the PBS and OPV+L groups ($p = 0.001$, 95% CI [0.789525, 1.045472]), but no significant differences were observed between the PBS and Vanco or PBS and OPV groups (Supplementary Table S9).

Similarly, in the *P. gingivalis* experiment, Levene's test showed significant heterogeneity of variances in the *P. gingivalis* group ($p = 0.007$, Supplementary Table S10). ANOVA results indicated significant differences between treatment groups ($F = 236.215$, $p < 0.001$, Supplementary Table S11). The post hoc test using Games-Howell

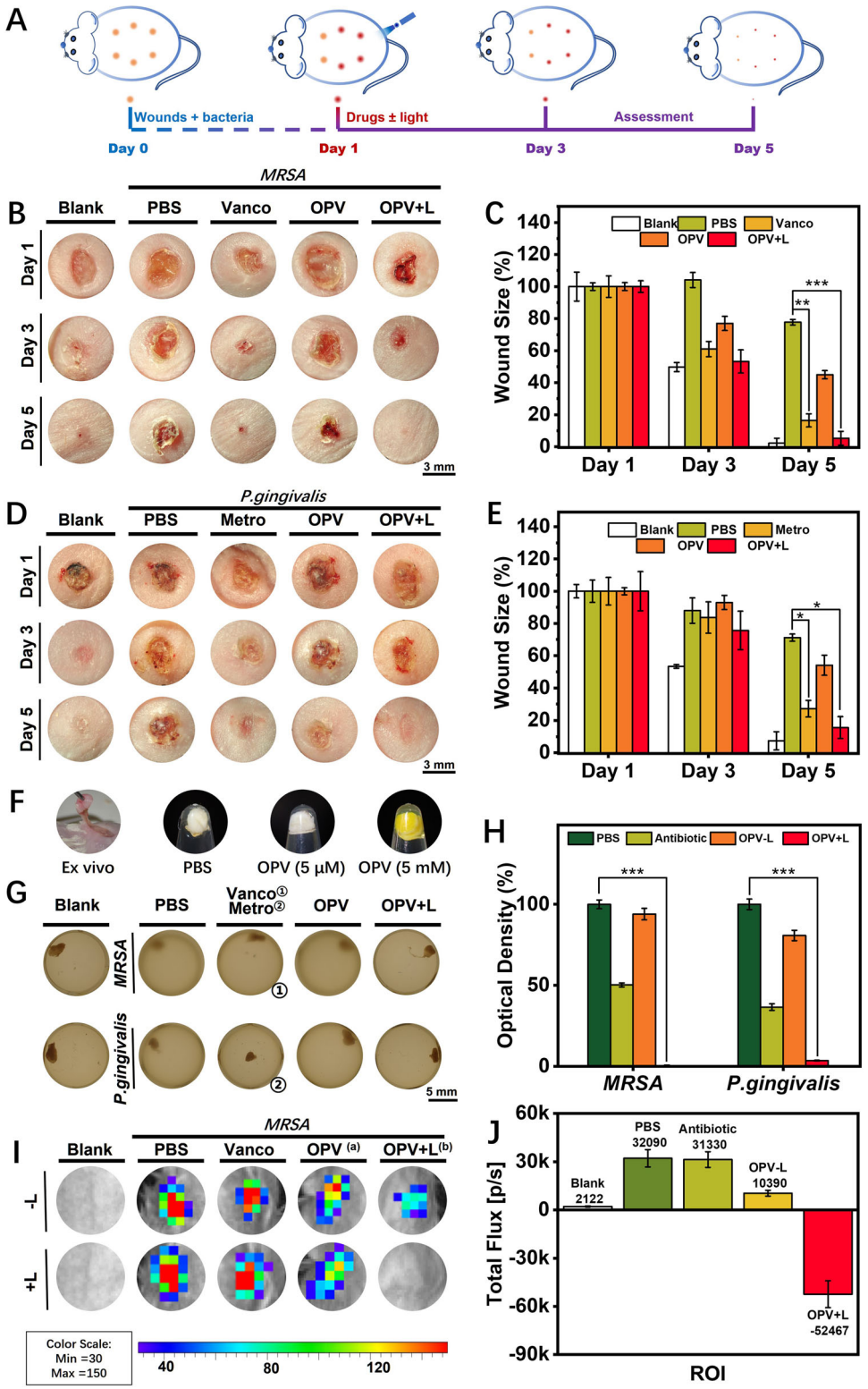

Fig. 5 (See legend on next page.)

(see figure on previous page)

Fig. 5 OPV and control groups acting on wounds in vivo and ex vivo. A Schematic illustration of the experimental procedures for the in vivo infection model. **B**, **D** Wound graphs of the no bacteria group or *MRSA*/*P. gingivalis* with the PBS, vancomycin/metronidazole, OPV, and OPV + light groups of mice. **C**, **E** Relative quantitative statistics of different groups of wound relative areas from (**B**) and (**D**), respectively. **F** Ex vivo image of skin tissue (φ: 3 mm) and drug incubation image with PBS or OPV (5 μM or 5 mM). **G** Ex vivo tissues incubated with *MRSA* or *P. gingivalis* in culture medium and killed by different treatments and (**H**) their relative quantitative statistics. **I** Fluorescence image of self-luminous *MRSA* with PBS, vancomycin, (a): Aluminum foil cover to prevent light exposure of OPV; (b): OPV+L exposed to light). **J** Relative fluorescence intensity changes before and after treatment (*$0.01 < p < 0.05$, **$0.001 < p < 0.01$, ***$p < 0.001$).

showed significant differences between the PBS and OPV+L groups ($p = 0.007$, 95% CI [0.52182268, 1.11990867]), but no significant differences were observed between the PBS and Metro groups and the PBS and OPV groups (Supplementary Table S12).

Experiment using real-time observations

To further demonstrate the immediate damage caused by OPV to bacteria, a local abscess experiment was conducted using our self-luminous *MRSA* contamination and the IVIS® Lumina III imaging system (Fig. 5I, J)[65]. The results showed significant differences in luminescence intensity among the different treatment groups, with the group treated with OPV+L and exposed to light having the lowest luminescence intensity. This indicates the most effective drug treatment and the strongest ability to quench bacterial luminescence.

Specifically, the luminescence intensity of the OPV+L group was 5363 with a standard deviation of 1085, which was lower than that of all other treatment groups. Compared to that of the group treated with PBS and exposed to light, the luminescence intensity of the OPV+L group was reduced by 94%. Compared to those of the groups treated with OPV and OPV+L, the luminescence intensity of the OPV+L group was reduced by 49%. Compared to the group with no drug treatment and no light exposure, the luminescence intensity of the OPV+L group was reduced by 98%. Therefore, it can be concluded that this drug treatment is the most effective at quenching bacterial luminescence (Supplementary Fig. S7).

Animal safety experiment

OPV was intravenously and locally injected into mice to compare the toxicity of PBS, and samples of five internal organs (e.g., heart, liver, spleen, lung, and kidney) were prepared by using histological hematoxylin and eosin (H&E) staining. There were no obvious differences (Supplementary Fig. S8).

OPV for other oral infections

Bacterial drug resistance is a problem in oral infections. Many oral bacteria have developed resistance to existing antibiotics, making the development of new antibiotics an important task. OPV can be chemically combined with antibiotics or other drugs to enhance their bacterial-killing effects and help solve the problem of drug resistance. For example, an *E. coli*-bound OPV-conjugated backbone combined with drugs can be used to kill tumor cells and may have good prospects for further application in the treatment of oral bacterial infections.

Bacteria can exist inside cells in oral infections, which makes them insensitive to traditional antibiotic treatments. However, OPV can enter cells and still effectively kill bacteria after modification. Therefore, OPV may become a new method for treating the internal existence of oral bacteria.

Oral bacteria can form biofilms, which are protective layers that are insensitive to traditional antibiotic treatments. Due to its molecular charge distribution and hydrophilic characteristics, OPV has an affinity for cell membranes and may be able to destroy the biofilms of oral bacteria, making them more susceptible to traditional antibiotic treatment.

Advantages of OPV over antibiotics or aPDT

In terms of antibacterial efficacy, OPV has several advantages over traditional aPDT or antibiotics.

Targeted and effective antibacterial effect

OPV can insert into bacterial cell membranes, allowing a more targeted and effective antibacterial effect compared to relying on electrostatic interactions.

Efficient excitation by blue light

OPV has a broad absorption range and can be efficiently excited by blue light, making it suitable for local infections such as periodontal disease and osteitis.

Low dark toxicity

OPV has low dark toxicity, allowing it to be added to infected tissues and penetrate before being exposed to light. This reduces the nonselective toxicity of disinfectants and antibiotics and allows for more precise targeting of infected areas.

Good biocompatibility and blood circulation safety

OPV has good biocompatibility and blood circulation safety, making it a safe method for topical use on local infections. It also has lower cytotoxicity than antibiotics when HaCaT cells are contaminated with *MRSA* or *P. gingivalis*.

Efficacy against drug-resistant bacteria

OPV has demonstrated efficacy against drug-resistant bacteria, including intracellular bacteria that traditional antibiotics may not effectively treat. This makes it a promising alternative for the treatment of drug-resistant infections.

Directions for future research

The limitations of this study include the lack of human clinical trials, the need for further optimization of OPV delivery and targeted treatment, the limited understanding of OPV pharmacokinetics and tissue distribution, the need for further investigation of the side effects and toxicity of OPV, the limited knowledge of the long-term effects of OPV treatment, the need for further exploration of the optimal light source and light dose for effective OPV treatment, and the limited understanding of its efficacy against different types of oral bacteria and their resistance mechanisms.

Future research can focus on the following directions to address these limitations:

1. The efficacy of OPV against different types of oral bacteria and their resistance mechanisms to expand its therapeutic scope.
2. The pharmacokinetics and tissue distribution of OPV to better understand its role in the human body.
3. Human clinical trials to evaluate the efficacy and safety of OPV for treating oral infections.

In addition, it is worth further investigating whether the use of OPV alone or in combination with lasers of other wavelengths can promote the migration and proliferation of periodontal ligament cells, the differentiation of osteoblasts, and anti-inflammatory effects[66–68].

Conclusions

OPV is an effective treatment option for periodontal disease, alveolar osteitis, and other superficial wound infections, as it can be efficiently activated using blue curing light in dental clinics. Due to its low dark toxicity, OPV can penetrate periodontal tissue before being exposed to light and can be applied at any time without causing nonselective toxicity. In contrast to antibiotics, OPV can target only the infected tissues, which are then exposed to a suitable light source to activate the OPV, making it an effective treatment against drug-resistant bacteria.

In summary, OPV effectively targets intracellular drug-resistant bacteria, addressing the two primary concerns of drug resistance and intracellular infection while reducing toxicity and drug resistance in nontreated areas, in contrast to traditional disinfectants and antibiotics. With numerous benefits and a wide range of potential applications, OPV shows significant promise for clinical use. Moreover, dental blue light curing lamps can successfully activate OPV, providing ample opportunities for future research on its clinical applications.

Acknowledgements

This work was supported by grants from the Fundamental Research Funds for the Central Universities-Peking University Medicine Fund of Fostering Young Scholars' Scientific & Technological Innovation (BMU2022PYB032) and the National Natural Science Foundation of China (52271127). We are deeply thankful for the help of Hongwei Jin from Peking University and Xiang Wang from the Chinese Academy of Forestry to support GROMACS, AutoDock Vina and Discovery Studio.

Author details

[1]Department of General Dentistry, Peking University School and Hospital of Stomatology, 100081 Beijing, P. R. China. [2]National Center for Stomatology & National Clinical Research Center for Oral Diseases & National Engineering Research Center of Oral Biomaterials and Digital Medical Devices, 100081 Beijing, P. R. China. [3]Beijing National Laboratory for Molecular Sciences, Key Laboratory of Organic Solids, Institute of Chemistry, Chinese Academy of Sciences, 100190 Beijing, P. R. China. [4]Department of Chemistry & Bioinspired Institute, Syracuse University, New York, USA. [5]Applied Oral Sciences and Community Dental Care, Faculty of Dentistry, The University of Hong Kong, Pokfulam, 999077 Hong Kong, P. R. China. [6]Center for Digital Dentistry, Peking University School and Hospital of Stomatology, 100081 Beijing, P. R. China. [7]First Clinical Division, Peking University School and Hospital of Stomatology, 100081 Beijing, P. R. China. [8]Department of Pediatric Dentistry, Peking University School and Hospital of Stomatology, 100081 Beijing, P. R. China

Author contributions

L.Y.: Designed and conducted all experiments, analyzed data, and wrote the main manuscript. X.F.: Synthesized the OPV material and assisted in experimental design and operation. W.Y.: Analyzed and tested the materials and assisted in experimental design and operation. H.W.: Assisted in molecular docking of the materials. F.D.: Cultured bacteria, performed in vivo fluorescence imaging, and conducted intracellular sterilization experiments. L.Z.: Cultured bacteria, performed extracellular sterilization experiments, and conducted animal safety experiments. G.W.: Detected excitation/emission peaks, performed photobleaching experiments and used zeta potential and flow cytometry for analysis. H.D.: Conducted cytotoxicity experiments and observed morphological changes. F.L.: Contributed to the experimental design and provided technical support. Y.W.: Provided funding and academic guidance and revised and approved the manuscript.

Conflict of interest

The authors declare no competing interests.

Supplementary information The online version contains supplementary material available at https://doi.org/10.1038/s41427-023-00487-8.

Received: 17 January 2023 Revised: 11 April 2023 Accepted: 30 May 2023.
Published online: 14 July 2023

References

1. Harris, A., Pineles, L. & Perencevich, E. Recognising the value of infection prevention and its role in addressing the antimicrobial resistance crisis. *BMJ Qual. Saf.* **26**, 683–686 (2017).
2. Shang, W. et al. Comparative fitness and determinants for the characteristic drug resistance of ST239-MRSA-III-t030 and ST239-MRSA-III-t037 strains isolated in China. *Micro. Drug Resist.* **22**, 185–192 (2016).
3. Matter, M. T. et al. Inorganic nanohybrids combat antibiotic-resistant bacteria hiding within human macrophages. *Nanoscale* **13**, 8224–8234 (2021).

4. Heil, E. L. & Tamma, P. D. Cefiderocol: the Trojan horse has arrived but will Troy fall? *Lancet Infect. Dis.* **21**, 153–155 (2021).
5. Butler, M. S. & Cooper, M. A. Antibiotics in the clinical pipeline in 2011. *J. Antibiot.* **64**, 413–425 (2011).
6. How, K. Y., Song, K. P. & Chan, K. G. *Porphyromonas gingivalis*: an overview of periodontopathic pathogen below the gum line. *Front. Microbiol.* **7**, 53 (2016).
7. Ye, P., Chang, J., Foo, L. F. & Yap, B. C. An early report: a modified porphyrin-linked metronidazole targeting intracellular *Porphyromonas gingivalis* in cultured oral epithelial cells. *Int. J. Oral. Sci.* **9**, 167–173 (2017).
8. Huang, X. et al. Microbial profile during pericoronitis and microbiota shift after treatment. *Front. Microbiol.* **11**, 1888 (2020).
9. Puidokas, T., Kubilius, M., Nomeika, D., Januzis, G. & Skrodeniene, E. Comparative analysis of blood clot, plasma rich in growth factors and platelet-rich fibrin resistance to bacteria-induced fibrinolysis. *Microorganisms* **7**, 328 (2019).
10. Tang, B. et al. Characteristics of oral methicillin-resistant *Staphylococcus epidermidis* isolated from dental plaque. *Int. J. Oral. Sci.* **12**, 15 (2020).
11. Lakhundi, S. & Zhang, K. Methicillin-resistant *Staphylococcus aureus*: molecular characterization, evolution, and epidemiology. *Clin. Microbiol. Rev.* **31**, e00020-18 (2018).
12. Zhu, H., Jin, H., Zhang, C. & Yuan, T. Intestinal methicillin-resistant *Staphylococcus aureus* causes prosthetic infection via 'Trojan Horse' mechanism: evidence from a rat model. *Bone Joint Res.* **9**, 152–161 (2020).
13. Li, R., Yuan, L., Jia, W., Qin, M. & Wang, Y. Effects of rose bengal- and methylene blue-mediated potassium iodide-potentiated photodynamic therapy on *Enterococcus faecalis*: a comparative study. *Lasers Surg. Med.* **53**, 400–410 (2021).
14. Yuan, L. et al. Potassium iodide enhances the photobactericidal effect of methylene blue on *Enterococcus faecalis* as planktonic cells and as biofilm infection in teeth. *J. Photochem. Photobiol. B* **203**, 111730 (2020).
15. Abrahamse, H. & Hamblin, M. R. New photosensitizers for photodynamic therapy. *Biochem. J.* **473**, 347–364 (2016).
16. Dai, T. et al. Blue light for infectious diseases: *Propionibacterium acnes*, *Helicobacter pylori*, and beyond? *Drug Resist. Updat.* **15**, 223–236 (2012).
17. Cai, Q. et al. Macrophage-instructed intracellular *Staphylococcus aureus* killing by targeting photodynamic dimers. *ACS Appl. Mater. Interfaces* **10**, 9197–9202 (2018).
18. Hu, F. et al. Visualization and in situ ablation of intracellular bacterial pathogens through metabolic labeling. *Angew. Chem. Int. Ed. Engl.* **59**, 9288–9292 (2020).
19. Oruba, Z. et al. Antimicrobial photodynamic therapy effectively reduces *Porphyromonas gingivalis* infection in gingival fibroblasts and keratinocytes: an in vitro study. *Photodiagnosis Photodyn. Ther.* **34**, 102330 (2021).
20. Soriano, J. et al. Cell death mechanisms in tumoral and non-tumoral human cell lines triggered by photodynamic treatments: apoptosis, necrosis and parthanatos. *Sci. Rep.* **7**, 41340 (2017).
21. Wang, H., Sun, P., Yin, L. & Sheng, X. 3D electronic and photonic structures as active biological interfaces. *InfoMat* **2**, 527–552 (2020).
22. Hu, P., He, X. & Jiang, H. Greater than 10 $cm^2 V^{-1} s^{-1}$: a breakthrough of organic semiconductors for field-effect transistors. *InfoMat* **3**, 613–630 (2021).
23. Xie, B., Chen, Z., Ying, L., Huang, F. & Cao, Y. Near-infrared organic photoelectric materials for light-harvesting systems: organic photovoltaics and organic photodiodes. *InfoMat* **2**, 57–91 (2020).
24. Peng, Q. et al. Recent advances in designing conductive hydrogels for flexible electronics. *InfoMat* **2**, 843–865 (2020).
25. Xu, M. K., Zhang, C., Zeng, Z. L. & Pu, K. Y. Semiconducting polymer nanoparticles as activatable nanomedicines for combinational phototherapy. *ACS Appl. Polym. Mater.* **3**, 4375–4389 (2021).
26. Li, J. C. & Pu, K. Y. Semiconducting polymer nanomaterials as near-infrared photoactivatable protherapeutics for cancer. *Acc. Chem. Res.* **53**, 752–762 (2020).
27. Praveen, V. K., Ranjith, C., Bandini, E., Ajayaghosh, A. & Armaroli, N. Oligo(-phenylenevinylene) hybrids and self-assemblies: versatile materials for excitation energy transfer. *Chem. Soc. Rev.* **43**, 4222–4242 (2014).
28. Nishizawa, T., Lim, H. K., Tajima, K. & Hashimoto, K. Efficient dyad-based organic solar cells with a highly crystalline donor group. *Chem. Commun.* **18**, 2469–2471 (2009).
29. Izawa, S., Hashimoto, K. & Tajima, K. Morphological stability of organic solar cells based upon an oligo(p-phenylenevinylene)-C70 dyad. *Phys. Chem. Chem. Phys.* **14**, 16138–16142 (2012).
30. Liu, S. et al. Electrochemiluminescence for electric-driven antibacterial therapeutics. *J. Am. Chem. Soc.* **140**, 2284–2291 (2018).
31. Yuan, H. et al. Chemical molecule-induced light-activated system for anticancer and antifungal activities. *J. Am. Chem. Soc.* **134**, 13184–13187 (2012).
32. Gao, Z. et al. Bacteria-mediated intracellular click reaction for drug enrichment and selective apoptosis of drug-resistant tumor cells. *ACS Appl. Mater. Interfaces* **14**, 12106–12115 (2022).
33. Zhou, L. et al. Cross-linking of thiolated paclitaxel-oligo(p-phenylene vinylene) conjugates aggregates inside tumor cells leads to "chemical locks" that increase drug efficacy. *Adv. Mater.* **30**, 1704888 (2018).
34. Nie, C. et al. Preparation of reactive oligo(p-phenylene vinylene) materials for spatial profiling of the chemical reactivity of intracellular compartments. *Adv. Mater.* **28**, 3749–3754 (2016).
35. Dai, N. et al. Fluorescent and biocompatible ruthenium-coordinated oligo(p-phenylenevinylene) nanocatalysts for transfer hydrogenation in the mitochondria of living cells. *Chemistry* **26**, 4489–4495 (2020).
36. Morales-de-Echegaray, A. V. et al. Antimicrobial photodynamic activity of gallium-substituted haemoglobin on silver nanoparticles. *Nanoscale* **12**, 21734–21742 (2020).
37. Dharmaratne, P. et al. Monosubstituted tricationic Zn(II) phthalocyanine enhances antimicrobial photodynamic inactivation (aPDI) of methicillin-resistant *Staphylococcus aureus* (MRSA) and cytotoxicity evaluation for topical applications: in vitro and in vivo study. *Emerg. Microbes Infect.* **9**, 1628–1637 (2020).
38. Sharma, M., Dube, A. & Majumder, S. K. Antibacterial photodynamic activity of photosensitizer-embedded alginate-pectin-carboxymethyl cellulose composite biopolymer films. *Lasers Med. Sci.* **36**, 763–772 (2021).
39. Van Der Spoel, D. et al. GROMACS: fast, flexible, and free. *J. Comput. Chem.* **26**, 1701–1718 (2005).
40. Humphrey, W., Dalke, A. & Schulten, K. VMD: visual molecular dynamics. *J. Mol. Graph.* **14**, 27–38 (1996).
41. Trott, O. & Olson, A. J. AutoDock Vina: improving the speed and accuracy of docking with a new scoring function, efficient optimization, and multithreading. *J. Comput. Chem.* **31**, 455–461 (2010).
42. Abraham, M. J. et al. GROMACS: high performance molecular simulations through multi-level parallelism from laptops to supercomputers. *SoftwareX* **1–2**, 19–25 (2015).
43. Berendsen, H., Postma, J. P. M., van Gunsteren, W. & Hermans, J. in *Intermolecular Forces. The Jerusalem Symposia on Quantum Chemistry and Biochemistry*, Vol. 14 (ed Pullman, B.) Interaction models for water in relation to protein hydration (Springer, 1981).
44. Kukol, A. Lipid models for united-atom molecular dynamics simulations of proteins. *J. Chem. Theory Comput.* **5**, 615–626 (2009).
45. Malde, A. K. et al. An Automated Force Field Topology Builder (ATB) and Repository: version 1.0. *J. Chem. Theory Comput.* **7**, 4026–4037 (2011).
46. Hoover, W. Canonical dynamics: equilibrium phase-space distributions. *Phys. Rev. A Mol. Opt. Phys.* **31**, 1695 (1985).
47. Nosé, S. & Klein, M. L. Constant pressure molecular dynamics for molecular systems. *Mol. Phys.* **50**, 1055–1076 (1983).
48. Okumura, H., Itoh, S. G., Nakamura, K. & Kawasaki, T. Role of water molecules and helix structure stabilization in the laser-induced disruption of amyloid fibrils observed by nonequilibrium molecular dynamics simulations. *J. Phys. Chem. B* **125**, 4964–4976 (2021).
49. Ponce, L. F., Montalvo, G., Leon, K. & Valiente, P. A. Differential effects of IL2Ralpha and IL15Ralpha over the stability of the common beta-gamma signaling subunits of the IL2 and IL15 receptors. *J. Chem. Inf. Model* **61**, 1913–1920 (2021).
50. Konermann, L., Aliyari, E. & Lee, J. H. Mobile protons limit the stability of salt bridges in the gas phase: implications for the structures of electrosprayed protein ions. *J. Phys. Chem. B* **125**, 3803–3814 (2021).
51. Kumar, S., Rosenberg, J. M., Bouzida, D., Swendsen, R. H. & Kollman, P. A. The weighted histogram analysis method for free-energy calculations on biomolecules. I. The method. *J. Comput. Chem.* **13**, 1011–1021 (1992).
52. Song, J., Peng, S., Yang, J., Zhou, F. & Suo, H. Isolation and identification of novel antibacterial peptides produced by *Lactobacillus fermentum* SHY10 in Chinese pickles. *Food Chem.* **348**, 129097 (2021).
53. Zhao, Y. et al. A biomimetic non-antibiotic approach to eradicate drug-resistant infections. *Adv. Mater.* **31**, e1806024 (2019).
54. Riyaphan, J., Pham, D. C., Leong, M. K. & Weng, C. F. In silico approaches to identify polyphenol compounds as alpha-glucosidase and alpha-amylase inhibitors against type-II diabetes. *Biomolecules* **11**, 1877 (2021).

55. Isenberg, G., Doerhoefer, S., Hoekstra, D. & Goldmann, W. H. Membrane fusion induced by the major lipid-binding domain of the cytoskeletal protein talin. *Biochem. Biophys. Res. Commun.* **295**, 636–643 (2002).
56. Vivcharuk, V. & Kaznessis, Y. N. Thermodynamic analysis of protegrin-1 insertion and permeation through a lipid bilayer. *J. Phys. Chem. B* **115**, 14704–14712 (2011).
57. Cowan, M. M., Van der Mei, H. C., Stokroos, I. & Busscher, H. J. Heterogeneity of surfaces of subgingival bacteria as detected by zeta potential measurements. *J. Dent. Res.* **71**, 1803–1806 (1992).
58. Teixeira, K. I., Cortes, M. E., Santos, R. A., Oliveira, F. & Sinisterra, R. D. KR12 peptide associated with cyclodextrin: antimicrobial and antitumor activities. *Biointerphases* **11**, 04B307 (2016).
59. Cios, A. et al. Effect of different wavelengths of laser irradiation on the skin cells. *Int. J. Mol. Sci.* **22**, 2437 (2021).
60. Austin, E. et al. Visible light. Part I: Properties and cutaneous effects of visible light. *J. Am. Acad. Dermatol.* **84**, 1219–1231 (2021).
61. Purbhoo-Makan, M., Houreld, N. N. & Enwemeka, C. S. The effects of blue light on human fibroblasts and diabetic wound healing. *Life* **12**, 1431 (2022).
62. Pourhajibagher, M., Ghorbanzadeh, R. & Bahador, A. Expression patterns of oxyR induced by oxidative stress from *Porphyromonas gingivalis* in response to photo-activated disinfection. *Infect. Drug Resist.* **11**, 717–725 (2018).
63. Lehar, S. M. et al. Novel antibody-antibiotic conjugate eliminates intracellular *S. aureus*. *Nature* **527**, 323–328 (2015).
64. MacArthur Clark, J. The 3Rs in research: a contemporary approach to replacement, reduction and refinement. *Br. J. Nutr.* **120**, S1–S7 (2018).
65. Yang, P. et al. 460nm visible light irradiation eradicates MRSA via inducing prophage activation. *J. Photochem. Photobiol. B* **166**, 311–322 (2017).
66. Liang, Y., Hu, Z., Li, Q. & Liu, X. Pyrophosphate inhibits periodontal ligament stem cell differentiation and mineralization through MAPK signaling pathways. *J. Periodontal Res.* **56**, 982–990 (2021).
67. Liang, Y., Shakya, A. & Liu, X. Biomimetic tubular matrix induces periodontal ligament principal fiber formation and inhibits osteogenic differentiation of periodontal ligament stem cells. *ACS Appl. Mater. Interfaces* **14**, 36451–36461 (2022).
68. Liang, Y., Luan, X. & Liu, X. Recent advances in periodontal regeneration: a biomaterial perspective. *Bioact. Mater.* **5**, 297–308 (2020).